nature neuroscience

Dnmt1 and Dnmt3a maintain DNA methylation and regulate synaptic function in adult forebrain neurons

Jian Feng[1], Yu Zhou[2,6], Susan L Campbell[3], Thuc Le[1,4], En Li[5], J David Sweatt[3], Alcino J Silva[2] & Guoping Fan[1]

Dnmt1 and Dnmt3a are important DNA methyltransferases that are expressed in postmitotic neurons, but their function in the CNS is unclear. We generated conditional mutant mice that lack *Dnmt1*, *Dnmt3a* or both exclusively in forebrain excitatory neurons and found that only double knockout (DKO) mice showed abnormal long-term plasticity in the hippocampal CA1 region together with deficits in learning and memory. Although we found no neuronal loss, hippocampal neurons in DKO mice were smaller than in the wild type; furthermore, DKO neurons showed deregulated expression of genes, including the class I MHC genes and *Stat1*, that are known to contribute to synaptic plasticity. In addition, we observed a significant decrease in DNA methylation in DKO neurons. We conclude that Dnmt1 and Dnmt3a are required for synaptic plasticity, learning and memory through their overlapping roles in maintaining DNA methylation and modulating neuronal gene expression in adult CNS neurons.

The long-lasting changes in synaptic plasticity that underlie learning and memory require changes in neuronal gene expression. Epigenetic mechanisms such as histone modification[1] and DNA methylation are thought to contribute to this adaptive neuronal gene expression[2–5]. Different histone modifications are associated with various neuronal gene expression states[1]; moreover, increasing histone acetylation by treatment with histone deacetylase inhibitors promotes recovery of learning and memory in a mouse model of neurodegeneration[6]. However, the function of DNA methylation in the adult nervous system is unclear. The substantial expression of the *de novo* DNA methyltransferase Dnmt3a and maintenance enzyme Dnmt1 in non-dividing neurons[7,8] is intriguing because these two enzymes normally establish and/or maintain DNA methylation patterns in fast-dividing cells. For instance, in dividing cells, Dnmt1 localizes to the replication foci and primarily methylates the unmethylated daughter strand DNA after DNA synthesis so that the parental DNA methylation pattern is maintained in the daughter cells. By contrast, Dnmt3a can establish new methylation patterns in unmethylated DNA regions, as seen in early mouse embryogenesis[9].

As mice with mutations in any of the three functional *Dnmt*s (*Dnmt1*, *Dnmt3a* and *Dnmt3b*) are not viable[9,10], conditional knockout mice have been generated to study the function of DNA methylation in the CNS[11–14]. Deletion of *Dnmt1* in neural progenitor cells causes hypomethylation in postmitotic neurons in the CNS (estimated at ~50% by high-performance liquid chromatography; data not shown). These mutant neural progenitor cells undergo precocious astroglial differentiation[15] and produce hypomethylated neurons with multiple defects in neuronal maturation and synaptic transmission[12,13]. Although these studies provide ample evidence that DNA methylation is essential in neuronal development and function, they do not reveal the role of continuous Dnmt expression in postmitotic neurons. Indeed, our study of conditional *Dnmt1* gene deletion in postmitotic CNS neurons failed to reveal any obvious neuronal phenotypes, such as a loss of DNA methylation in cultured cerebellar neurons or cortical and hippocampal neurons *in vivo*[11]. Nevertheless, we did observe a moderate effect on cortical neuronal survival in a rodent model of stroke when Dnmt1 was reduced by 50% in postmitotic cortical and hippocampal neurons[16].

Recently, studies with Dnmt inhibitors in *in vitro* brain slices or hippocampus *in vivo*[4,17,18] have indicated that DNA methylation might target specific genes involved in synaptic plasticity and learning and memory. However, the potential toxic effects of Dnmt inhibitors on protein translation in non-dividing neurons could complicate the interpretation of those results[19]. The lack of selectivity of Dnmt inhibitors also makes it difficult to correlate specific neural effects with individual Dnmts. Unlike histone modifications, DNA methylation is presumably a more static epigenetic mark and whether DNA methylation undergoes turnover in postmitotic neurons is still under debate[20]. Nevertheless, evidence of selective DNA demethylation in a subset of neuronal gene promoters[2,21–23] in the CNS argues for the presence of demethylation activity in neurons.

There is also circumstantial evidence that the *de novo* methyltransferases Dnmt3a and Dnmt3b are important for neural development and function. ICF (or immunodeficiency, centromere instability and facial anomalies) syndrome, a rare human disorder, is caused by a recessive mutation of the *DNMT3B* gene[9,24]. A significant portion

[1]Department of Human Genetics and [2]Department of Neurobiology, David Geffen School of Medicine, University of California Los Angeles, Los Angeles, California, USA. [3]Department of Neurobiology, University of Alabama at Birmingham, Birmingham, Alabama, USA. [4]Interdepartmental Neuroscience Program, David Geffen School of Medicine, University of California Los Angeles, Los Angeles, California, USA. [5]Epigenetics Program, Novartis Institutes for Biomedical Research, Cambridge, Massachusetts, USA. [6]Present address: Department of Physiology, Medical College of Qingdao University, Qingdao, China. Correspondence should be addressed to G.F. (gfan@mednet.ucla.edu).

Received 14 December 2009; accepted 15 February 2010; published online 14 March 2010; doi:10.1038/nn.2514

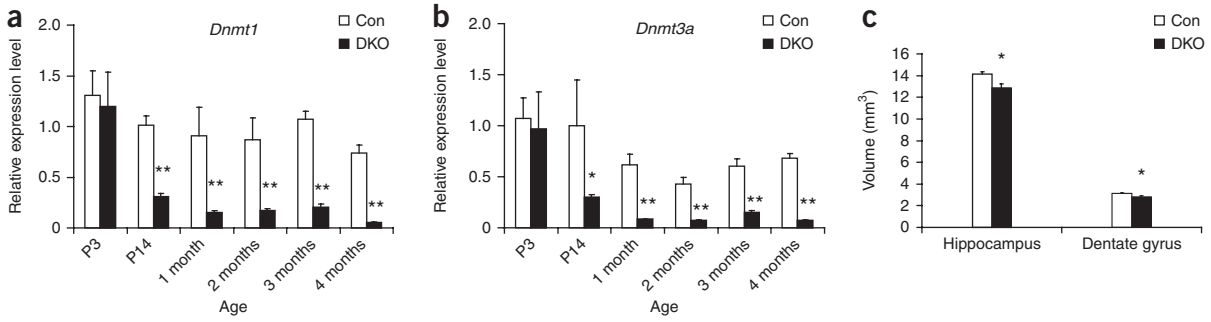

Figure 1 Mice with conditional deletion of *Dnmt1* and *Dnmt3a* have small hippocampi without cell loss. (**a**,**b**) Relative expression of *Dnmt1* (**a**) and *Dnmt3a* (**b**) in hippocampi of DKO and wild-type littermate control (Con) mice were compared at various postnatal ages. Three pairs of samples were used for each postnatal age. (**c**) Stereological analysis of the volume of hippocampus and dentate gyrus in DKO and control mice. Data are presented as mean ± s.e.m. $*P < 0.05$, $**P < 0.01$.

of ICF patients suffer mental retardation. Gene expression studies have shown that *Dnmt3b* is highly expressed in the murine neural tube between embryonic day (E)7.5 and E9.5 (ref. 9), indicating that Dnmt3b might have a role in early stages of neurogenesis. We have shown that Dnmt3a is present in both developing and mature CNS[7], indicating that it might be involved in the regulation of DNA methylation in both embryonic and adult CNS neurons. Conditional mutant mice lacking Dnmt3a in the entire CNS (*Nes-Cre1; Dnmt3a*) are born apparently normal but die in young adulthood[14]. These *Nes-Cre1; Dnmt3a* mutant mice showed a loss of motor neurons in the hypoglossal nucleus and morphological defects in the neuromuscular junctions of the diaphragm, indicating that Dnmt3a contributes to the survival of motor neurons and the maintenance of neuromuscular endplate structure[14].

In this study, we compare the phenotypes of conditional mutant mice that are deficient for Dnmt1, Dnmt3a or both exclusively in the forebrain postnatal postmitotic neurons. We aim to address whether Dnmt1 and Dnmt3a have a redundant role in the maintenance of DNA methylation pattern in postmitotic neurons. Furthermore, we determine the effects of Dnmt deficiencies on neuronal gene expression, synaptic function, and learning and memory.

RESULTS

Deficits in cell size and neural plasticity in DKO mice

Calcium/calmodulin-dependent protein kinase IIα (CamKIIα) is expressed in postmitotic neurons postnatally[25]. We therefore used the *Camk2a* promoter-driven Cre recombinase (*Camk2a-Cre93*) to induce *Dnmt* gene deletion in postmitotic neurons in the CNS. This *Camk2a-Cre93* transgene can induce specific gene deletion in excitatory neurons in the mouse forebrain shortly after birth because its expression peaks within 2–3 weeks postnatally[11]. Our previous study with a conditional deletion of *Dnmt1* in postmitotic neurons did not show any significant alteration in DNA methylation in repetitive elements[11]. To determine whether Dnmt1 and Dnmt3a have redundant roles in the CNS, we made *Dnmt1* and *Dnmt3a* double conditional knockouts (DKO) in addition to single *Dnmt1* or *Dnmt3a* conditional knockouts (SKO). Consistent with the CamKIIα expression pattern, *Dnmt1* and *Dnmt3a* gene deletion was not detected at postnatal day 3 (P3) (**Fig. 1a**,**b**). However, by P14 the levels of *Dnmt* transcripts were significantly decreased and remained low beyond P30 (**Fig. 1a**,**b**). Immunostaining of Cre recombinase in DKO confirmed that Cre expression was restricted to mature neurons, which is consistent with previous findings showing neuron-specific conditional gene deletion by the *Camk2a-Cre93* transgene[11] (**Supplementary Fig. 1**). Southern blot analysis also confirmed that the efficiency of the *Dnmt* gene deletion (**Supplementary Fig. 1**) was at a constant level (~50% from 1 to 4 months old, as reported)[11].

DKO mice have normal lifespans and show no obvious behavioral defects in their home cages. On gross histological examination, all brain structures appeared intact (**Supplementary Fig. 2**). Using stereological protocols, we measured hippocampal volumes in control and mutant mice. Although we found no abnormalities in the brains of SKO mice (data not shown), DKO mice had significantly smaller hippocampi (9.31% average volume reduction, $P < 0.05$) than did control mice (control: 14.16 ± 0.19 mm^3; DKO: 12.84 ± 0.41 mm^3 (mean ± s.e.m.); $P < 0.05$; **Fig. 1c**). The dentate gyrus in DKO mice showed a similar volume reduction (9.77% on average; control: 3.12 ± 0.07 mm^3; DKO: 2.82 ± 0.11 mm^3 (mean ± s.e.m.); $P < 0.05$; **Fig. 1c**). These observations indicate that the reduction in volume of the hippocampus is directly proportional to the reduction in volume of the dentate gyrus in DKO mice. We used an unbiased optical fractionator and found that the total number of dentate gyrus granule cells is similar between DKO and control mice (control: 427.87 ± 44.10; DKO: 443.72 ± 34.40 (mean ± s.e.m.); $P > 0.05$; $n = 5$ for control and $n = 6$ for DKO). However, quantitative measurement of individual neuronal volume in the dentate gyrus indicated that DKO neurons were significantly smaller than those of control mice (control: 280.08 ± 6.98 μm^3; DKO: 254.95 ± 7.17 μm^3 (mean ± s.e.m.); $P < 0.05$; $n = 5$ for control and $n = 6$ for DKO). The dentate gyrus is one of the two CNS regions in which adult neurogenesis occurs. We performed an adult neurogenesis assay by BrdU labeling of adult neural stem cells and newly born neurons in the dentate gyrus and found no difference in neurogenesis between DKO and control mice (**Supplementary Fig. 2**). Together, our results indicate that the difference in hippocampal volume between control and DKO mice is probably due to a reduction in the size of DKO neurons.

Next, we investigated the effect of Dnmt1 and Dnmt3a deficiency in forebrain excitatory neurons on synaptic function. We first examined hippocampal plasticity in Schaffer collateral–CA1 synapses. We studied CA1 long-term potentiation (LTP) and long-term depression (LTD) in littermate control, DKO and SKO mice. The late phase of Schaffer collateral LTP induced by 100-Hz tetanus was significantly attenuated ($P < 0.05$) in DKO mice (**Fig. 2a** and data not shown). In addition, DKO mice showed enhanced induction of LTD using a stimulation protocol (1 Hz for 15 min) that normally fails to induce LTD in adult wild-type mice ($P < 0.05$; **Fig. 2b**). By contrast, SKO mice showed neither LTP nor LTD abnormalities (**Supplementary Fig. 3**). Basal synaptic transmission does not differ between DKO mice and controls, as shown by plotting varying stimulus intensity (10–100 μA) against the presynaptic fiber volley amplitudes and postsynaptic

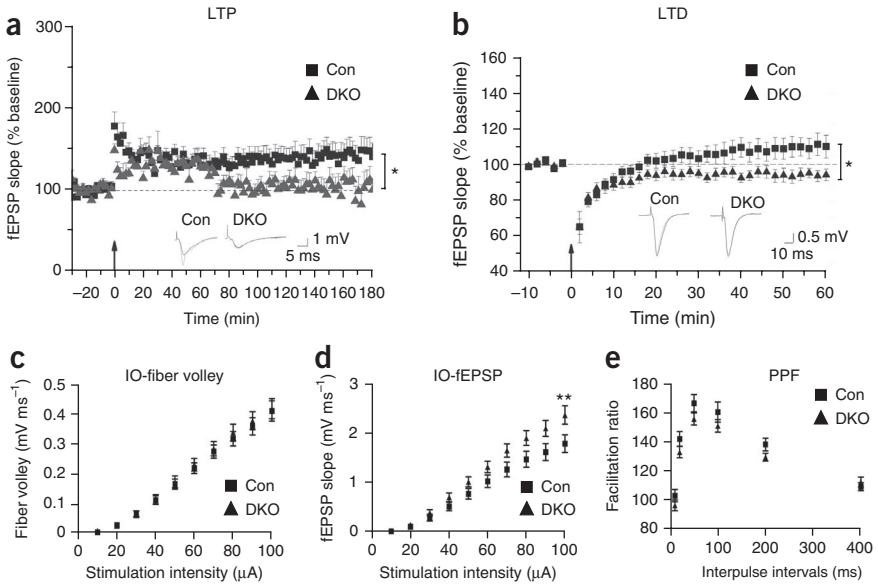

Figure 2 Impaired neural plasticity in DKO mice. (**a**) Field EPSP (fEPSP) slopes in control (squares) versus DKO mice (triangles) recorded before and after tetanic stimulation (100 Hz, 1 s, twice with 20-s interval). $*P < 0.05$. $n = 28$ slices from 9 control mice; $n = 13$ slices from 7 DKO mice. (**b**) LTD was enhanced in adult DKO mice. fEPSP slopes were recorded before and after stimulation (1 Hz, 15 min). $*P < 0.05$. $n = 10$ slices from 5 control mice and $n = 8$ slices from 4 DKO mice. Representative recordings are shown in insets (**a**,**b**). (**c**,**d**) The basal synaptic transmission from the DKO and control mice are identical, as shown by plotting varying stimulus intensity (10–100 μA) against the presynaptic fiber volley amplitudes (**c**) and postsynaptic fEPSP slope (**d**). $n = 33$ slices from 8 DKO mice and $n = 28$ slices from 8 control mice. (**e**) PPF studies across different ISIs revealed no difference between DKO and control mice. $n = 16$ slices from 4 DKO mice and $n = 14$ slice from 4 control mice. Slice numbers were used for statistical analysis. Data are presented as mean ± s.e.m.

fEPSP slopes (**Fig. 2c**,**d**). Paired-pulse facilitation (PPF) studies across different inter-stimulus intervals (ISIs) revealed no differences between DKO and control mice (**Fig. 2e**). Although it is still unclear whether the abnormalities in synaptic plasticity are mediated by pre- or postsynaptic mechanisms, our data indicate that Dnmt1 and Dnmt3a are required for normal synaptic plasticity.

Deficits in hippocampal learning and memory in DKO mice

As deficits in CA1 LTP are known to disrupt spatial learning, we next tested the mice on the hidden-platform version of the Morris water maze, a hippocampus-dependent learning and memory task. In this task, animals were trained to search for a submerged platform in a pool of water. After 4, 8 and 12 days of training (2 trials per day), we assessed spatial learning using probe trials in which the platform was removed from the pool, and the mice were allowed to search for 60 s (**Fig. 3a**). Although *Dnmt1* and *Dnmt3a* SKO mice performed normally in this task (**Supplementary Fig. 4**), DKO mice took longer to find the platform during training ($P < 0.05$, two-way ANOVA; **Fig. 3b**). When the platform was removed during the probe trials, DKO mice spent less time in the target quadrant than did littermate controls ($P < 0.05$; **Fig. 3c**), indicating impaired spatial learning and memory ability. However, the swimming speeds of DKO and control mice were not significantly different from each other (**Fig. 3d**).

Having determined that DKO mice show deficits in hippocampus-dependent memory, we performed contextual fear-conditioning tests to investigate the acquisition and consolidation of memory. Although control and DKO mice behaved similarly in terms of memory acquisition (IM test; **Fig. 3e**,**f**), DKO mice showed an impairment in memory consolidation (24-h test; **Fig. 3f**). We found no behavioral defects in *Dnmt1* or *Dnmt3a* SKO mice in the fear-conditioning test (**Supplementary Fig. 5**). This is consistent with the idea that Dnmt1 and Dnmt3a have redundant roles in the regulation of learning and memory in adult animals.

Upregulation of *MHC I*, *Stat1* and other genes in DKO brain

Changes in gene expression are required for the late stages of long-term plasticity and for learning and memory consolidation. Previous studies have indicated that *Reln* and *PP1*, both of which are associated with learning and memory, are modulated by DNA methylation. Furthermore, infusion of the Dnmt inhibitors 5′–azadeoxylcytidine and zebularine paired with behavioral memory training triggers

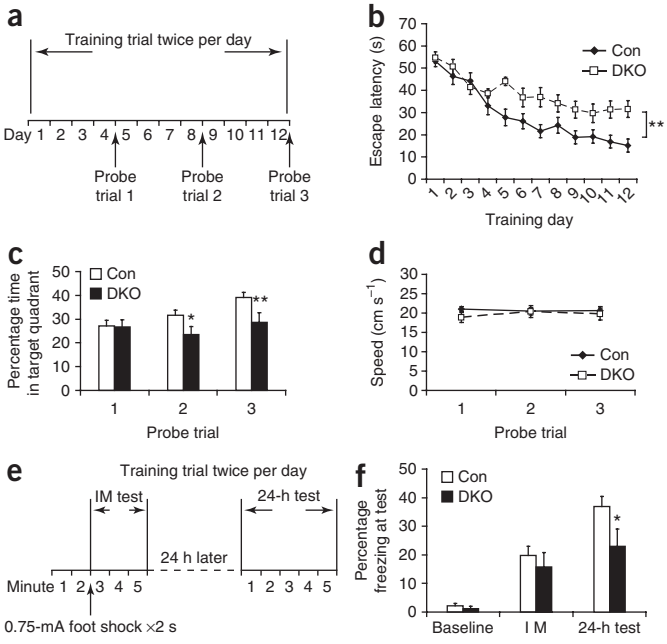

Figure 3 Impaired learning and memory in DKO mice. (**a**–**d**) Morris water maze test. (**a**) Schematic drawing of the Morris water maze test design. (**b**) Escape latency (time to find the hidden platform) plotted against training day. Genotype $F(1, 30) = 6.25$, $P = 0.019$, two-way ANOVA. (**c**) Percentage time spent in target quadrant during three probe trials. (**d**) Swimming speeds measured in DKO ($n = 13$) and control ($n = 17$) mice. Three-month-old mice were used in **b**–**d**. (**e**–**f**) Contextual fear conditioning test. (**e**) Schematic drawing of the contextual fear conditioning test design. Mice were trained and tested immediately (IM/average for 3 min) and 24 h later in a conditioning chamber. (**f**) Contextual memory consolidation was measured by freezing frequency at 24 h. The acquisition was normal in DKO immediately after shock. Baseline, freezing before shock presentation; IM, freezing immediately after shock presentation. $n = 21$ DKO and $n = 13$ control mice in **f**. Data are presented as mean ± s.e.m. $*P < 0.05$; $**P < 0.01$.

Table 1 List of upregulated genes in DKO mouse brain

Gene symbol	Accession ID	Gene name	Fold contrast
MHC I-mediated immunity			
B2m	NM_009735	Beta-2 microglobulin	3
H2-D	AK083376	Clone:C920025E04 product: weakly similar to H-2 CLASS I HISTOCOMPATIBILITY ANTIGEN, D-37 ALPHA CHAIN PRECURSOR	2.32
H2-D1	NM_010380	Histocompatibility 2, D region locus 1	3.14
H-2K	NM_019909	MHC (A.CA/J(H-2K-f) class I antigen (LOC56628)	3.34
H-2K(b)	U47328	MHC class I heavy chain precursor	2.15
H2-M2	AY302216	Strain P/J MHC class Ib antigen	1.94
H2-M3	NM_013819	Histocompatibility 2, M region locus 3	1.93
H2-Q1	NM_010390	Histocompatibility 2, Q region locus 1	2.54
H2-Q5	NM_010393	Histocompatibility 2, Q region locus 5	2.4
H2-Q7	NM_010394	Histocompatibility 2, Q region locus 7	2.85
H2-Q8	NM_023124	Histocompatibility 2, Q region locus 8	3.9
H2-T23	NM_010398	Histocompatibility 2, T region locus 23	2.4
MHC class I	M28684	MHC class I Tla-37-like mRNA, partial cds	2.56
mRNA transcription regulation			
Sox21	NM_145464	SRY-box containing gene 21	2.79
Stat1	NM_009283	Signal transducer and activator of transcription 1	1.91
Interferon-related immunity			
Cxcl10	NM_021274	Chemokine (C-X-C motif) ligand 10	9.71
Gbp2	NM_010260	Guanylate nucleotide binding protein 2	3.44
Gbp4	NM_018734	Guanylate nucleotide binding protein 4	3.81
Ifi1	NM_008326	Interferon inducible protein 1	2.8
Ifi27	NM_029803	Interferon, alpha-inducible protein 27	3.66
Ifi44	NM_133871	Interferon-induced protein 44	3.23
Ifi47	NM_008330	Interferon gamma inducible protein 47	3.15
Ifi204	NM_008329	Interferon activated gene 204	3.04
Ifitm7	NM_028968	Interferon induced transmembrane protein 7	2.04
Igtp	NM_018738	Interferon gamma induced GTPase	5.55
Iigp1	NM_021792	Interferon inducible GTPase 1	7.23
Iigp2	NM_019440	Interferon inducible GTPase 2	5
Oas1f	NM_145153	2′-5′ oligoadenylate synthetase 1F	2.56
Oasl2	NM_011854	2′-5′ oligoadenylate synthetase-like 2	5.55
Complement-mediated immunity			
C3	NM_009778	Complement component 3	3.85
C4	NM_009780	Complement component 4 (within H-2S)	3.64
Cell communication and others			
Ccl5	NM_013653	Chemokine (C-C motif) ligand 5	4.05
Ccl12	NM_011331	Chemokine (C-C motif) ligand 12	2.51
Cxcl5	BC033508	Chemokine (C-C motif) ligand 5, mRNA (cDNA clone MGC:35989 IMAGE:4925413)	3.35
Lgals3bp	NM_011150	Lectin, galactoside-binding, soluble, 3 binding protein	2.71
Mell1	NM_013783	Mel transforming oncogene-like 1	1.73
Mgl1	NM_010796	Macrophage galactose N-acetyl-galactosamine specific lectin 1	2.03
Xlr	NM_011725	X-linked lymphocyte-regulated complex	1.94
Xlr4	NM_021365	X-linked lymphocyte-regulated 4	2.79

the upregulation of these two genes[17,18]. We therefore performed quantitative real-time (qRT)-PCR analysis to determine whether the expression of *Reln* and *PP1* is altered in the absence of both Dnmt1 and Dnmt3a. However, we found that the expression of these genes is normal in DKO hippocampi, indicating that alterations in the expression of these two genes are not the basis for the abnormalities in synaptic plasticity and learning and memory in DKO animals (**Supplementary Fig. 6**). To identify novel target genes that are deregulated in the forebrains of DKO mice, we performed microarray analysis of genome-wide gene expression. Bioinformatics analysis showed that 84 genes (0.26%) were upregulated more than 1.5-fold, whereas 7 genes (0.02%) showed more than 1.5-fold downregulation.

Gene-expression analysis of the DKO cortex showed that the highly upregulated genes are immune genes including *MHC I* and those involved in the complement system, as well as *Stat1*, a signaling molecule that is activated during interferon-gamma triggered immune responses (**Table 1**). All these genes are important for synaptic function in the CNS and for learning and memory[26–28]. *In situ* hybridization showed that neuronal cells have enhanced *MHC I* transcripts (**Fig. 4a**). The upregulated expression of *MHC I* and other immune genes was confirmed by qRT-PCR in adult hippocampi (**Fig. 4b**) and cortical tissues (data not shown). The induction of these immune genes seems to be a direct consequence of Dnmt1 and Dnmt3a deficiency in neuronal cells because the change in expression was noticed soon after the completion of *Camk2a-cre*–mediated deletion of *Dnmt1* and *Dnmt3a* two weeks postnatally (**Fig. 4d**), but not at P3 when *Dnmt* deletion was not complete (**Figs. 1a**,**b** and **4c**). Single *Dnmt1* or *Dnmt3a* conditional mutant mice showed no significant changes in expression of these genes compared to controls (**Supplementary Fig. 7**), indicating that Dnmt1 and Dnmt3a have redundant roles in repressing these genes in neuronal cells.

To determine whether conditional deletion of *Dnmt1* and *Dnmt3a* leads to cell-autonomous upregulation of *MHC I* and other immune molecules in the CNS, we examined gene expression in pure $Dnmt1^{2lox/2lox}$; $Dnmt3a^{2lox/2lox}$ hippocampal neuronal cultures by conditionally deleting both *Dnmt1* and *Dnmt3a* with the infection of

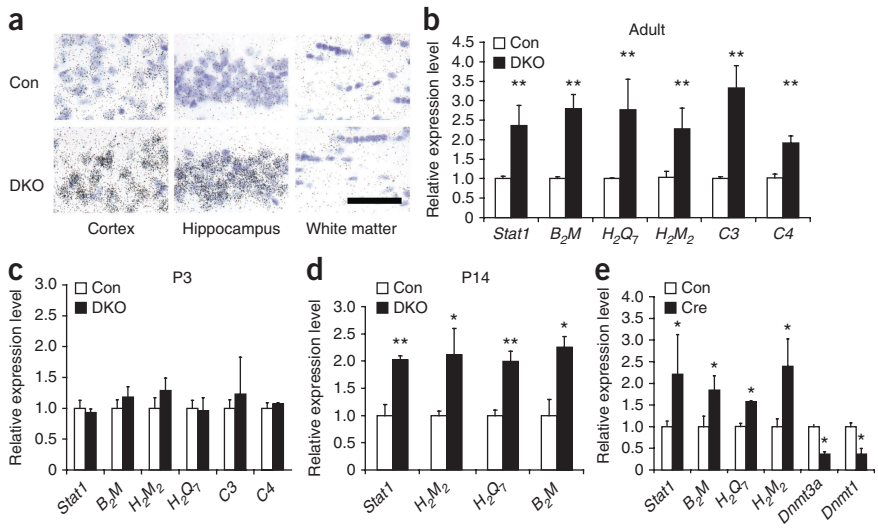

Figure 4 Induction of immune genes in DKO mouse brain. (**a**) Neuronal induction of *MHC I* gene expression in DKO. *In situ* hybridization of H_2D was post-stained with cresyl violet to reveal the nuclei. Silver grains appeared black. In the cortex and hippocampus of DKO mice, *MHC I* signal is highly concentrated in the neurons whose nuclei are large and lightly stained with cresyl violet. By contrast, in the white matter, where most cells are glia whose nuclei are small and dark stained, there was no significant difference compare to controls. Scale bar at bottom right, 100 μm, applies to all panels. (**b**) Real-time PCR analysis of the immune genes *Stat1*, B_2M, H_2M_2, H_2Q_7, *C3* and *C4* in hippocampi of 2–3 months adults. (**c**,**d**) The induction of immune genes in the hippocampus was found as early at P14 (**d**) but not at P3 (**c**). n = 3–4 pairs of samples for each experiment. (**e**) Real-time PCR analysis of *Stat1*, B_2M, H_2M_2 and H_2Q_7 as well as expression of *Dnmt3a* and *Dnmt1* in $Dnmt1^{2lox/2lox}Dnmt3a^{2lox/2lox}$ mouse hippocampal neuronal cultures 5 d after adeno-cre virus infection. Hippocampal neuronal culture with adeno-GFP viruses infection was used as control. Data are presented as mean ± s.e.m. $^*P < 0.05$; $^{**}P < 0.01$.

adeno-cre viruses (**Fig. 4e**). We found that deficiency of both Dnmt1 and Dnmt3a in pure hippocampal neuron cultures also induced upregulation of *MHC I* and other immune genes. Thus, our data indicate that the upregulation of *MHC I* molecules in DKO forebrain neurons is probably a cell-intrinsic event.

Demethylation of neuronal genes in DKO forebrain neurons

Using phosphor-Stat1 immunohistochemistry[28], we found that the active form of Stat1 was also concentrated in neuronal cell types in DKO mouse brain (**Fig. 5a**). The neuronal upregulation of *Stat1* and *MHC I*-related immune genes in the forebrains of DKO mice could be due to a direct effect of promoter demethylation as a consequence of Dnmt1 and Dnmt3a deficiency or to an indirect cause involving transcriptional regulators of immune genes. We first examined whether DNA demethylation occurs in postmitotic neurons in the cortex and hippocampus of the DKO mice by looking at the candidate gene *Stat1*, which is involved in regulating neural plasticity[28] and in the interferon (IFN) pathway that mediates the induction of *MHC I* expression in neurons[29]. We previously showed that *Stat1* expression is repressed by DNA methylation[15]. We therefore performed bisulfite sequencing analysis of the *Stat1* promoter region. Although the methylation level at −400 to −750 bp of the *Stat1* promoter was similar between DKO and control mice (**Supplementary Fig. 8**), we found a demethylated domain at −895 to −1,010 bp of the *Stat1* promoter in DKO mice (**Fig. 5b**). Interestingly, *Dnmt* SKO mice showed no decrease in methylation in the *Stat1* promoter (**Supplementary Fig. 8**), consistent with the notion that Dnmt1 and Dnmt3a compensate for each other in maintaining DNA methylation in SKO mice. We also found that DNA demethylation in this *Stat1* promoter domain in DKO mice occurs as early as P14, when deletion of both *Dnmt1* and *Dnmt3a* is just complete (**Fig. 5c**). This result indicates that Dnmt1 and Dnmt3a are required for maintaining DNA methylation in CNS neurons from an early postnatal stage.

To determine whether demethylation in the *Stat1* gene promoter is exclusive to neuronal populations, we isolated nuclei positive for the

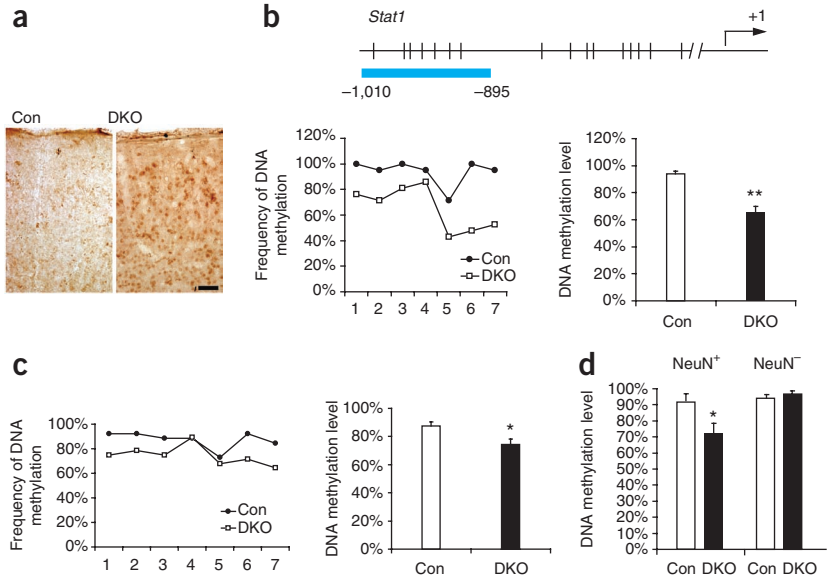

Figure 5 Stat1 protein increase in DKO mouse brain in conjunction with promoter demethylation in neuronal cells. (**a**) Immunohistochemistry of DKO cortex showing increase phosphorylated Stat1, mainly in cells with neuronal shapes. Scale bar, 50 μm, applies to both panels. (**b**) Bisulfite sequencing of *Stat1* promoter of control and DKO forebrains at 3 months old. Schematic gene promoter structure is shown with each CpG site marked with a vertical slash. The blue bar highlights the promoter region subject to methylation analysis. A summary of methylation frequency at individual CpG sites is shown in a line chart and the mean of DNA methylation levels of individual alleles is shown in bar chart[23]. (**c**) Bisulfite sequencing of *Stat1* promoter showed enhanced DNA demethylation within DKO tissue at P14. (**d**) Bisulfite sequencing of *Stat1* promoter of FAC-sorted NeuN positive and negative nucleus sub-populations from DKO and control mouse forebrains. Here the demethylation of *Stat1* promoter is restricted to $NeuN^+$ DKO cells. We analyzed 30 clones from 3 samples. Data are presented as mean ± s.e.m. Unpaired student *t*-test; $^*P < 0.05$, $^{**}P < 0.01$.

neuronal marker NeuN through NeuN live staining and fluorescence-activated cell sorting (FACS) for methylation analysis (**Supplementary Fig. 9**). Consistent with the neuron-specific deletion of the *Dnmt* genes, significant demethylation appeared only in neuronal populations with the NeuN marker and not in NeuN-negative controls cells (**Fig. 5d**).

Having seen selective demethylation in the *Stat1* gene promoter in DKO but not SKO mice, we decided to quantify potential reductions in total DNA methylation in DKO cortex and hippocampus through mass spectrometry analysis. We found that DKO cortex and hippocampus showed approximately 20% reduction in total methylcytosine levels ($n = 4$, $P < 0.01$; **Fig. 6a**), indicating that demethylation in DKO neurons is widespread. Consistently, *Dnmt* SKO brain DNAs showed no significant decrease in the total methylcytosine level (**Supplementary Fig. 10**), consistent with the idea that Dnmt1 and Dnmt3a have complementary roles in the maintenance of DNA methylation in the CNS.

To systematically identify what kind of neuronal genes are significantly demethylated in DKO forebrain neurons, we carried out a DNA methylation profiling experiment using methylated DNA immunoprecipitation (MeDIP). Using 5-methylcytosine antibodies for DNA immunoprecipitation and cross-hybridization to Agilent promoter arrays (covering 15,561 proximal gene regions mainly at −800 bp to +200 bp)[30], we identified 161 candidate loci that would exhibit demethylation (based on established criteria[30]: Log2 > 0.2 and *t*-test $P < 0.01$ of hybridization signals of control and DKO tissues; **Supplementary Table 1**). Using PANTHER classification categories (http://www.pantherdb.org), gene ontology analysis indicated that these 161 loci were enriched within promoters of genes of cytokine signaling, signal transduction or oxidoreductase gene categories (**Fig. 6b**). We noticed that the 161 potentially demethylated promoters did not overlap with the list of 84 genes that are upregulated in DKO mice. We suspect that the minimal overlap could be due to the

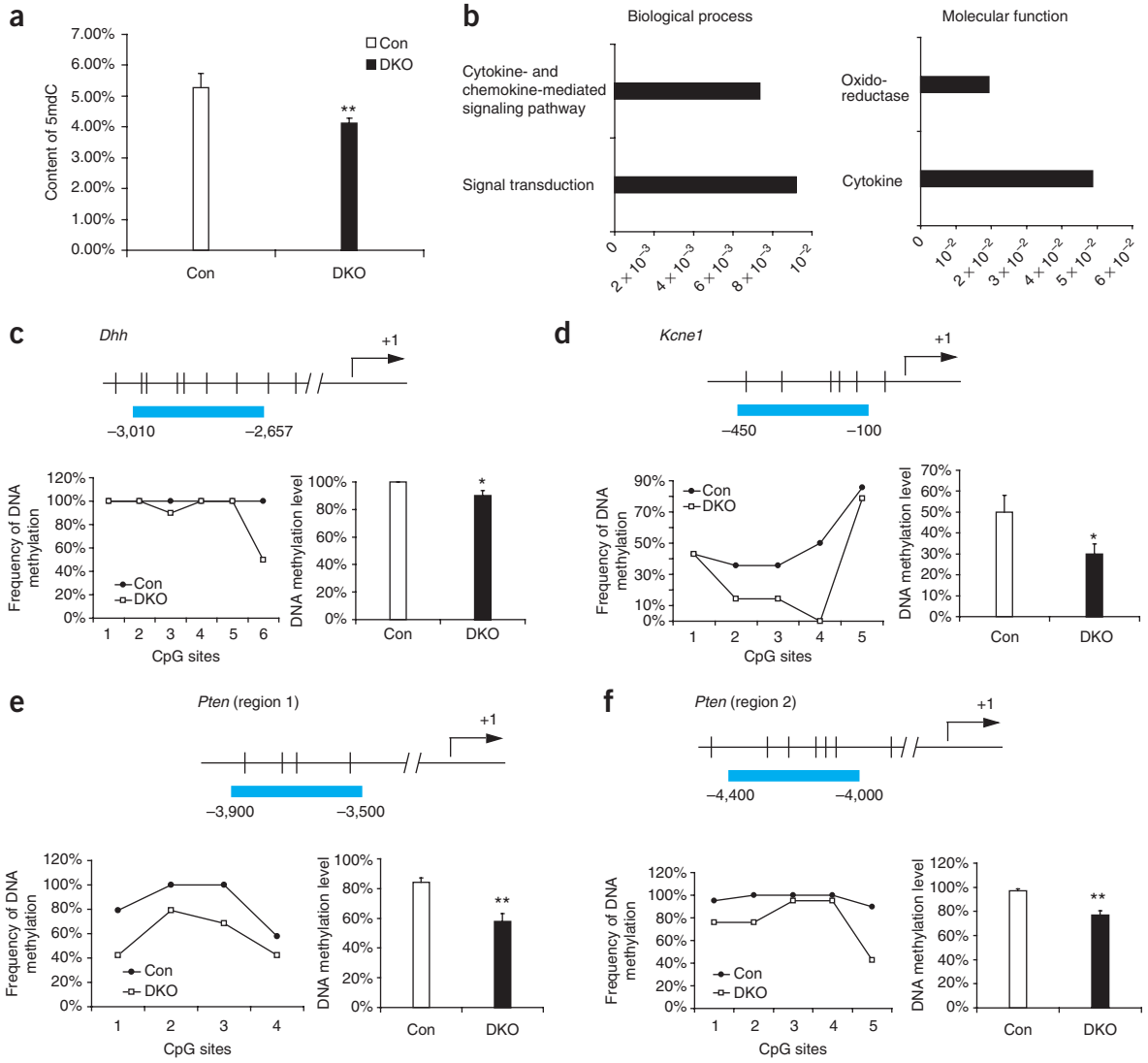

Figure 6 Gene ontology and bisulfite sequencing verification of MeDIP-chip analysis. (**a**) Quantitative analysis of 5-methylcytosine using liquid chromatography–electrospray ionization tandem mass spectrometry (LC-ESI-MS/MS) 5-Methylcytosine content is expressed as the percentage of 5-methylcytosine in the total cytosine pool. Data are the mean ± s.e.m. from replicates of four separate experiments ($n = 16$). (**b**) Gene ontology classifications of MeDIP–chip result based on categories of biological process and molecular function plotted against the *P* value of enrichment significance. (**c**–**f**) Four gene loci (*Dhh* (**c**), *Kcne1* (**d**), *Pten* region 1 (**e**) and *Pten* region 2 (**f**)) were verified for DNA demethylation. The results are displayed in the same manner as in **Figure 5**. Data as shown were from DKO and control mouse forebrains at 2–3 months old. Data are presented as mean ± s.e.m. Unpaired student *t*-test; $*P < 0.05$, $**P < 0.01$.

technical limitations of the current MeDIP microarray, which was not sensitive enough to detect all demethylated regions. In addition, our promoter microarray mainly focused on the −800 bp to +200 bp proximal gene promoter regions, potentially missing out many more demethylated domains outside this 1-kb region. A perfect case is the absence of the corresponding array probe for the −895 to −1,010 bp domain on the *Stat1* promoter, whose demethylation is correlated with an increase in *Stat1* mRNA. In addition, promoter demethylation itself might not be sufficient to cause gene upregulation, as in the case of *Dnmt1*$^{-/-}$ embryonic stem cells[30]. Finally, the MeDIP assay measures methylation in the population of all nuclei in the forebrain, which might not be correlated with the potential change in gene expression in a small subset of cortical and hippocampal neurons in DKO mice.

Nevertheless, the identification of a list of potentially demethylated gene promoters allowed us to validate whether selective demethylation takes place in a subset of neuronal gene promoters. We therefore selected eight candidate genes for the confirmation of methylation changes. The choice of these eight genes was based on the potential roles for these genes in neuronal signaling or ion-channel functions. We found that six gene promoters (75% accuracy) showed demethylation changes in DKO mouse brain (**Fig. 6c–f** and unpublished data, J.F. and T.L.). Specifically, *Kcne1, Dhh* and *Pten* (analyzed in two regions) each showed 10–30% less methylation in DKO mice when compared with littermate control mice (three pairs). Together with mass spectrometry data, our MeDIP and bisulfite sequencing analysis support the notion that Dnmt1 and Dnmt3a are essential for keeping proper methylation patterns at certain genomic loci of postmitotic CNS neurons.

DISCUSSION

By conditionally deleting *Dnmt1* and *Dnmt3a* exclusively in postnatal postmitotic neurons, our experiments provided the first direct evidence that DNA methyltransferases are required for the maintenance of neuronal DNA methylation, for proper control of gene expression, and consequently for synaptic plasticity, as well as learning and memory. Because *Dnmt1* or *Dnmt3a* SKOs do not show the defects seen in DKOs, our results show that Dnmt1 and Dnmt3a have redundant roles in postmitotic neurons. Previously, the overlapping functions of different members of the Dnmts were observed in fast-dividing cancer cell lines or mouse embryonic stem cells. For example, DNMT3B and DNMT1 are known for their cooperative role in maintaining DNA methylation in colon cancer cells[31]. In mouse embryonic stem cells, Dnmt1 cooperates with Dnmt3a and Dnmt3b to maintain DNA methylation[32,33]. In dividing cells, Dnmt1 is concentrated in the replicating foci during S-phase to maintain DNA methylation following DNA synthesis. Dnmt3a and Dnmt3b frequently associate with heterochromatin regions and co-localize with heterochromatin protein 1α (HP1) in a cell cycle-independent manner[34]. However, the localization of Dnmt1 and Dnmt3a in postmitotic CNS neurons appears to be in a diffuse pattern[7] (our unpublished data) as neuronal cells are arrested at the G0 phase of the cell cycle. How Dnmt1 and Dnmt3a carry out an overlapping function is still unclear. It is possible that Dnmt1 and Dnmt3a are co-localized or in the same methylation complex to maintain methylation patterns in postmitotic neurons. Alternatively, either Dnmt1 or Dnmt3a alone can recognize newly demethylated CpGs and carry out re-methylation function. Future studies with genome-wide location analysis of Dnmt1, Dnmt3a or Dnmt complexes in adult CNS neurons might resolve this question.

Our results show that Dnmt1 and Dnmt3a deficiency in forebrain neurons causes defects in synaptic plasticity as well as learning and memory. In humans, mutations in DNA methylation machinery are associated with mental retardation disorders. The notable examples include *DNMT3B* mutations for ICF syndrome and *MECP2* mutations for Rett syndrome[2,3,5,9,24]. Thus, identifying the crucial learning and memory genes that are affected by Dnmt1 and Dnmt3a deficiency in mutant mice would be beneficial to our understanding of human disorders. Among those genes that are deregulated in DKO mice, we suspect that upregulation of immune genes, such as *class I MHC*[26] and *Stat1*[28], in neurons might be relevant to the defects in learning and memory identified here. Neurophysiological abnormalities associated with MHC I-deficient mice have been reported, including enhanced LTP and loss of LTD[26,35]. The DKO phenotype in this study includes upregulation of immune genes, loss of LTP and facilitated LTD, which is opposite to what has been observed in MHC I-deficient mice. In addition, the proposed roles of immune molecules in neuronal dendrite pruning and elimination[35,36] are also consistent with our current observation that neurons in the DKO mouse brain are smaller than those of controls, which could be the result of a defect in dendritic pruning. It is still unclear how Dnmt1 and Dnmt3a deficiency in the forebrain leads to upregulation of *MHC I* and other immune genes. We note that demethylation-induced *MHC I* gene expression also takes place in cultured fibroblasts, indicating that DNA hypomemethylation-mediated *MHC I* upregulation is not unique to postmitotic neurons[37]. *MHC I* expression can be activated in neurons through the interferon gamma (IFNγ) pathway[29]. Our finding that the *Stat1* gene is demethylated and upregulated in Dnmt-deficient neurons is consistent with the possibility that the cytokine signaling pathway might be involved in MHC I upregulation in hypomethylated neurons.

Our study showed that DNA demethylation takes place in postmitotic neurons in the absence of both Dnmt1 and Dnmt3a *in vivo*. How DNA demethylation takes place in postmitotic neurons is also uncertain. In plants, a DNA glycocylase-based demethylation mechanism has been identified. In mammals, several DNA demethylation pathways have been proposed (for example, via MBD2[38], Gadd45a[39] and Gadd45b[23]) and the most likely pathway for DNA demethylation in non-dividing neurons seems to be through base-excision repair. Indeed, it has been proposed that Dnmt1 in neuronal cells has a role in the maintenance of DNA methylation after DNA repair[40]. In neuronal cells, high levels of oxidative stress can cause oxidative deamination of 5′methylcytosine (5mdC), leading to G:T mismatch. The G:T mismatch can activate the DNA base-excision/repair pathway and subsequently result in unmethylated C:G base pairing. More recently, it has been shown that neurons, but not non-neuronal cells, contain 5′hydroxyl-methylcytosine (5hmdC)[41]. The production of 5hmdC results from the oxidation of 5′methylcytosine (5mdC) by Tet1 enzymes[42]. We found that levels of total 5mdC and 5hmdC in control and DKO brain tissues are proportional to the total 5mdC levels (**Supplementary Fig. 10**), supporting the notion that 5hmdC is derived from hydroxylation of 5mdC substrate. A possible DNA demethylation pathway would involve a repair mechanism to convert 5hmdC into cytosine. Considering our findings that Dnmt1 and Dnmt3a have a redundant role in CNS neurons, we suggest that either Dnmt1 or Dnmt3a can prevent potential demethylation in neurons caused by DNA oxidation/repair pathways.

METHODS

Methods and any associated references are available in the online version of the paper at http://www.nature.com/natureneuroscience/.

Accession codes. Microarray data are available at GEO (Gene Expression Omnibus, http://www.ncbi.nlm.nih.gov/prejects/geo/index.cgi) with accession number GSE19367.

Note: Supplementary information is available on the Nature Neuroscience website.

ACKNOWLEDGMENTS

We thank X.-H. Lu and X.W. Yang for help with stereology analysis, T. Chailangkarn and S. Fouse for technical support and P. Golshani for critical reading of the paper. We also thank all members of the Fan laboratory for help and advice. Funding was provided by grants from the US National Institutes of Health to G.F. (RO1 NS051411), A.J.S. (P50-MH0779720) and J.D.S. (AG031722, MH57014 and NS057098). G.F. is a Carol Moss Spivak Scholar in Neuroscience.

AUTHOR CONTRIBUTIONS

The studies were directed by G.F. and conceived and designed by J.F. and G.F. G.F., A.J.S. and J.D.S. coordinated the project. J.F. performed the behavioral tests, morphology analysis, gene expression and DNA methylation analysis. Y.Z. performed the fear-conditioning test, LTD and synaptic transmission experiments. S.L.C. performed the LTP experiments. T.L. carried out DNA hydrolysis/LC-ESI-MS/MS experiments and contributed to the DNA methylation analysis. E.L. contributed *Dnmt3a*$^{2lox/2lox}$ mice. The paper was written by J.F. and G.F. and was commented on by all the authors.

COMPETING FINANCIAL INTERESTS

The authors declare no competing financial interests.

Published online at http://www.nature.com/natureneuroscience/.
Reprints and permissions information is available online at http://www.nature.com/reprintsandpermissions/.

1. Tsankova, N., Renthal, W., Kumar, A. & Nestler, E.J. Epigenetic regulation in psychiatric disorders. *Nat. Rev. Neurosci.* **8**, 355–367 (2007).
2. Martinowich, K. *et al.* DNA methylation-related chromatin remodeling in activity-dependent BDNF gene regulation. *Science* **302**, 890–893 (2003).
3. Chen, W.G. *et al.* Derepression of BDNF transcription involves calcium-dependent phosphorylation of MeCP2. *Science* **302**, 885–889 (2003).
4. Nelson, E.D., Kavalali, E.T. & Monteggia, L.M. Activity-dependent suppression of miniature neurotransmission through the regulation of DNA methylation. *J. Neurosci.* **28**, 395–406 (2008).
5. Feng, J., Fouse, S. & Fan, G. Epigenetic regulation of neural gene expression and neuronal function. *Pediatr. Res.* **61**, 58R–63R (2007).
6. Guan, J.S. *et al.* HDAC2 negatively regulates memory formation and synaptic plasticity. *Nature* **459**, 55–60 (2009).
7. Feng, J., Chang, H., Li, E. & Fan, G. Dynamic expression of de novo DNA methyltransferases Dnmt3a and Dnmt3b in the central nervous system. *J. Neurosci. Res.* **79**, 734–746 (2005).
8. Goto, K. *et al.* Expression of DNA methyltransferase gene in mature and immature neurons as well as proliferating cells in mice. *Differentiation* **56**, 39–44 (1994).
9. Okano, M., Bell, D.W., Haber, D.A. & Li, E. DNA methyltransferases Dnmt3a and Dnmt3b are essential for *de novo* methylation and mammalian development. *Cell* **99**, 247–257 (1999).
10. Li, E., Bestor, T.H. & Jaenisch, R. Targeted mutation of the DNA methyltransferase gene results in embryonic lethality. *Cell* **69**, 915–926 (1992).
11. Fan, G. *et al.* DNA hypomethylation perturbs the function and survival of CNS neurons in postnatal animals. *J. Neurosci.* **21**, 788–797 (2001).
12. Golshani, P., Hutnick, L., Schweizer, F. & Fan, G. Conditional Dnmt1 deletion in dorsal forebrain disrupts development of somatosensory barrel cortex and thalamocortical long-term potentiation. *Thalamus Relat. Syst.* **3**, 227–233 (2005).
13. Hutnick, L.K. *et al.* DNA hypomethylation restricted to the murine forebrain induces cortical degeneration and impairs postnatal neuronal maturation. *Hum. Mol. Genet.* **18**, 2875–2888 (2009).
14. Nguyen, S., Meletis, K., Fu, D., Jhaveri, S. & Jaenisch, R. Ablation of *de novo* DNA methyltransferase Dnmt3a in the nervous system leads to neuromuscular defects and shortened lifespan. *Dev. Dyn.* **236**, 1663–1676 (2007).
15. Fan, G. *et al.* DNA methylation controls the timing of astrogliogenesis through regulation of JAK-STAT signaling. *Development* **132**, 3345–3356 (2005).
16. Endres, M., Fan, G., Meisel, A., Dirnagl, U. & Jaenisch, R. Effects of cerebral ischemia in mice lacking DNA methyltransferase 1 in post-mitotic neurons. *Neuroreport* **12**, 3763–3766 (2001).
17. Miller, C.A. & Sweatt, J.D. Covalent modification of DNA regulates memory formation. *Neuron* **53**, 857–869 (2007).
18. Levenson, J.M. *et al.* Evidence that DNA (cytosine-5) methyltransferase regulates synaptic plasticity in the hippocampus. *J. Biol. Chem.* **281**, 15763–15773 (2006).
19. Jüttermann, R., Li, E. & Jaenisch, R. Toxicity of 5-aza-2′-deoxycytidine to mammalian cells is mediated primarily by covalent trapping of DNA methyltransferase rather than DNA demethylation. *Proc. Natl. Acad. Sci. USA* **91**, 11797–11801 (1994).
20. Ooi, S.K. & Bestor, T.H. The colorful history of active DNA demethylation. *Cell* **133**, 1145–1148 (2008).
21. Weaver, I.C. *et al.* Epigenetic programming by maternal behavior. *Nat. Neurosci.* **7**, 847–854 (2004).
22. Weaver, I.C. *et al.* Reversal of maternal programming of stress responses in adult offspring through methyl supplementation: altering epigenetic marking later in life. *J. Neurosci.* **25**, 11045–11054 (2005).
23. Ma, D.K. *et al.* Neuronal activity-induced Gadd45b promotes epigenetic DNA demethylation and adult neurogenesis. *Science* **323**, 1074–1077 (2009).
24. Xu, G.L. *et al.* Chromosome instability and immunodeficiency syndrome caused by mutations in a DNA methyltransferase gene. *Nature* **402**, 187–191 (1999).
25. Ouimet, C.C., McGuinness, T.L. & Greengard, P. Immunocytochemical localization of calcium/calmodulin-dependent protein kinase II in rat brain. *Proc. Natl. Acad. Sci. USA* **81**, 5604–5608 (1984).
26. Huh, G.S. *et al.* Functional requirement for class I MHC in CNS development and plasticity. *Science* **290**, 2155–2159 (2000).
27. Stevens, B. *et al.* The classical complement cascade mediates CNS synapse elimination. *Cell* **131**, 1164–1178 (2007).
28. Tropea, D. *et al.* Gene expression changes and molecular pathways mediating activity-dependent plasticity in visual cortex. *Nat. Neurosci.* **9**, 660–668 (2006).
29. Neumann, H., Schmidt, H., Cavalie, A., Jenne, D. & Wekerle, H. Major histocompatibility complex (MHC) class I gene expression in single neurons of the central nervous system: differential regulation by interferon (IFN)-gamma and tumor necrosis factor (TNF)-alpha. *J. Exp. Med.* **185**, 305–316 (1997).
30. Fouse, S.D. *et al.* Promoter CpG methylation contributes to ES cell gene regulation in parallel with Oct4/Nanog, PcG complex, and histone H3 K4/K27 trimethylation. *Cell Stem Cell* **2**, 160–169 (2008).
31. Rhee, I. *et al.* DNMT1 and DNMT3b cooperate to silence genes in human cancer cells. *Nature* **416**, 552–556 (2002).
32. Chen, T., Ueda, Y., Dodge, J.E., Wang, Z. & Li, E. Establishment and maintenance of genomic methylation patterns in mouse embryonic stem cells by Dnmt3a and Dnmt3b. *Mol. Cell. Biol.* **23**, 5594–5605 (2003).
33. Liang, G. *et al.* Cooperativity between DNA methyltransferases in the maintenance methylation of repetitive elements. *Mol. Cell. Biol.* **22**, 480–491 (2002).
34. Bachman, K.E., Rountree, M.R. & Baylin, S.B. Dnmt3a and Dnmt3b are transcriptional repressors that exhibit unique localization properties to heterochromatin. *J. Biol. Chem.* **276**, 32282–32287 (2001).
35. Boulanger, L.M. & Shatz, C.J. Immune signaling in neural development, synaptic plasticity and disease. *Nat. Rev. Neurosci.* **5**, 521–531 (2004).
36. Perry, V.H. & O'Connor, V. C1q: the perfect complement for a synaptic feast? *Nat. Rev. Neurosci.* **9**, 807–811 (2008).
37. Jackson-Grusby, L. *et al.* Loss of genomic methylation causes p53-dependent apoptosis and epigenetic deregulation. *Nat. Genet.* **27**, 31–39 (2001).
38. Bhattacharya, S.K., Ramchandani, S., Cervoni, N. & Szyf, M. A mammalian protein with specific demethylase activity for mCpG DNA. *Nature* **397**, 579–583 (1999).
39. Barreto, G. *et al.* Gadd45a promotes epigenetic gene activation by repair-mediated DNA demethylation. *Nature* **445**, 671–675 (2007).
40. Brooks, P.J., Marietta, C. & Goldman, D. DNA mismatch repair and DNA methylation in adult brain neurons. *J. Neurosci.* **16**, 939–945 (1996).
41. Kriaucionis, S. & Heintz, N. The nuclear DNA base 5-hydroxymethylcytosine is present in Purkinje neurons and the brain. *Science* **324**, 929–930 (2009).
42. Tahiliani, M. *et al.* Conversion of 5-methylcytosine to 5-hydroxymethylcytosine in mammalian DNA by MLL partner TET1. *Science* **324**, 930–935 (2009).

ONLINE METHODS

Transgenic mice. Generation of *Dnmt1*$^{2lox/2lox}$ mice has been described[11]. The *Dnmt3a*$^{2lox/2lox}$ mice were generated at Novartis Institutes of Biomedical Research[43]. They were backcrossed with 129Jae mice for several generations to generate a common genetic background. We crossed *Dnmt1*$^{2lox/2lox}$ mice with *Dnmt3a*$^{2lox/2lox}$ mice to produce *loxP*-flanked *Dnmt1* and *Dnmt3a* homozygous offspring. Subsequent matings of three kinds of Dnmt floxed homozygotes with *Camk2a-cre* mice lead to *Camk2a-cre; Dnmt1*$^{2lox/2lox}$*Dnmt3a*$^{2lox/2lox}$ double knockout (DKO), *Camk2a-cre; Dnmt1*$^{2lox/2lox}$, and *Camk2a-cre; Dnmt3a*$^{2lox/2lox}$ single knockout (SKO) and *Camk2a-cre* negative littermate control. The animal protocols used in the studies here were approved by the UCLA Institutional Animal Research Committee.

Real-time PCR analysis. Total RNA was extracted using Trizol reagent (Invitrogen). RNA samples (1 μg) were treated with DNase I (Invitrogen) and reverse transcription was performed using iScript RT kit (Bio-Rad). The SybrGreen supermix kit (Bio-Rad) was used for real-time PCR. Threshold cycle (Ct) was determined on the linear phase. Results were normalized by Ct of 18 s. Relative gene expression fold difference was calculated by $2^{-\Delta\text{normalized Ct}}$. PCR primers are listed in **Supplementary Table 2**.

Immunohistochemistry. Immunohistochemistry was carried out as described[7]. The primary antibodies used in this experiment were rabbit anti-Cre (Covance, 1:3,000) and mouse anti-NeuN (Chemicon, 1:300). Activated phosphor-Stat1 (Abcam, 1:500) immunohistochemistry was also performed as described[28].

Southern blot analysis. DNA samples were extracted from brain tissues, and 10 μg DNA samples were digested by SpeI restriction enzyme, were subjected to electrophoresis and transferred to a positive-charged Hybond membrane. The DNA probe[11] was labeled with ^{32}P dCTP using the Prime-It II Random Primer Labeling Kit (Stratagene). Hybridization was performed with the Quickhyb kit (Stratagene). PhosphorImager was used for hybridization detection.

BrdU labeling. BrdU (Sigma) was injected intraperitoneally every two hours for five injections at 10 mg per kg body weight. Twelve hours after the first injection, the mice were cardiac perfused with 4% paraformaldehyde. Then they were post-fixed and cryoprotected as usual. Sections were cut and stained for BrdU antibody by using Vectastain Elite ABC kits (Vector) with DAB as substrate. The BrdU$^+$ cells at the subgranular zone of the dentate gyrus were counted as described[44]. In brief, four sections from each mouse at comparable rostrocaudal levels were counted. Four mice per genotype were used.

Stereology. We cut 40-μm-thick coronal sections of hippocampi. A series of sections (10–12 sections per brain; 240 μm apart or 1 in 6) were randomly picked. The slides were mounted and went through cresyl violet staining. The structures were then traced and contoured under a 5× objective. The volume was determined using the Cavalieri protocol (StereoInvestigator; MicroBrightField). The absolute granule cell number was also estimated using an optical fractionator as described[45]. Counting frames of 15 μm × 15 μm × 40 μm were used in a 100 μm × 100 μm matrix and were randomly superimposed onto the dentate gyrus. The nucleator program was used for neuronal cell body size measurement as described[46]. The counting frame used was 15 μm × 15 μm and the sampling grid was 100 μm × 100 μm. The coefficient of sampling error (Gundersen's CE, $m = 1$) was used to determine the precision of the estimates or sampling variation within each brain. The CE was controlled to be less than 0.10.

Electrophysiology. Animals were killed using a guillotine. The brain was immersed in ice-cold cutting saline before isolation of the caudal portion containing the hippocampus and entorhinal cortex. Transverse slices (400 μm) were prepared with a Vibratome. After isolation, cortical tissue was removed and hippocampal slices were equilibrated in a mixture of 50% cutting saline and 50% artificial cerebrospinal fluid (ACSF) at room temperature. Slices were further equilibrated in 100% ACSF for 45 min at room temperature, followed by a final incubation in 100% ACSF at 32 °C for 1 h. All solutions were saturated with 95%/5% O_2/CO_2. Electrophysiology was performed in an interface chamber. Oxygenated ACSF was perfused into the recording chamber at 1 ml min^{-1}. Electrophysiological traces were digitized and stored using Digidata and Clampex software (Axon Instruments). Extracellular stimuli were administered on the border of areas CA3 and CA1 along the Schaffer collaterals. fEPSPs were recorded in the stratum radiatum. The relationship between fiber volley and fEPSP slopes over various stimulus intensities was used to assess baseline synaptic transmission. All subsequent experimental stimuli were set to an intensity that evoked a fEPSP that had a slope of 50% of the maximum fEPSP slope. Slices were stimulated for at least 10 min to generate baseline values before LTP or LTD induction. LTP was induced with 1 pair of 100-Hz tetani (1 s each, separated by 20 s). LTD was elicited with a 1-Hz protocol (900 pulses, 15 min). The results were analyzed by two-way ANOVA with repeated measures. *Post-hoc* comparisons after two-way ANOVA were made using the method of Bonferroni.

For synaptic transmission experiments, all test stimuli and tetanus pulses were 100 μs in duration and 1/2–2/3 maximal stimulation strength. For measurement of PPF, we used different ISIs. Statistical comparisons were made with *n* indicating the number of slices.

Morris water maze behavioral test. During the training trials of the hidden-platform version of the Morris water maze test, the platform location was fixed and submerged under opaque water. Mice were trained with two trials per day (1 min per trial) for 12 days. During each trial, the mouse was released into the water maze at a pseudo-random starting position. The trial ended when either the mouse climbed onto the platform or a maximum of 60 s elapsed. The mouse was then kept on the platform for 5 s. A 60-s probe test was conducted at the end of training on days 4, 8 and 12, in which the platform was removed from the pool.

Contextual fear conditioning. Training consisted of placing the mice in a conditioning chamber and presenting a shock (2 s, 0.75 mA) 2 min later. Mice remained in the chamber for an additional 3 min. The mice were placed back in the same chamber and tested for contextual fear conditioning 24 h later. Our index of memory, freezing (the cessation of all movement except for respiration), was assessed by an automated scoring system (Med Associates) with a 30 frames per s sampling; freezing was counted if the mouse froze continuously for 1 s or more.

Microarray analysis. Forebrains (cortex and hippocampus) from gender–matched, 2–3-month-old mice were used for total RNA measurement using Trizol. Antisense RNAs (cRNAs) were converted and fluorescently labeled using an Agilent low RNA input fluorescent linear amplification kit according to the manufacturer's instructions. The resulting labeled cRNA probes were combined and hybridized to the same Agilent 44K mouse gene expression array. The hybridization was stopped after 17 h of incubation at 65 °C with rotation speed at 4 rpm. The slides were washed and scanned. The resultant data were retrieved by Agilent feature extraction software 8.5 and analyzed by FOCUS software.

***In situ* hybridization.** Riboprobes were labeled with [α-^{35}S]UTP using the riboprobe combination system kit (Promega) and then purified with the RNeasy Kit (Qiagen). The probe plasmid was a gift from S. Nelson (University of California Los Angeles, Los Angeles, California, USA). Cryostat sections (15 μm) were washed/incubated in the following series of solutions at room temperature: 0.1 M glycine in 0.1M PB; 0.1M PB; acetic anhydride/TEA buffer; SSC; 50, 70, 95, and 100% ethanol solutions; chloroform; 100 and 95% ethanol. Then probes were added onto the slides. Hybridized slides were incubated at 60 °C overnight. Slides were then washed in series of SSC solutions and rinsed in water. Hybridized slides were pressed against a film for 4–5 days before dipping in Kodak NTB2 emulsion. Following exposure to emulsion at 4 °C the slides were developed, stained with cresyl violet, attached to coverslips, and photographed.

Hippocampal neuron cultures and adeno-virus infection. Mouse hippocampal neurons were isolated at E15.5 as described[47]. The culture dishes were coated with poly-DL-ornithine and laminin. The hippocampal neurons were cultured in Neurobasal medium supplemented with glutamine, antibiotics and B27 (Invitrogen). The hippocampal cultures were infected with adeno-cre virus at 3 days *in vitro* (DIV) with adeno-GFP virus infection as control[11].

Methylation analysis. Genomic DNA was digested by BglII enzyme and treated with sodium bisulfite[7]. After DNA cleaning with Wizard DNA cleanup kit (Promega), either nested or touchdown PCRs were carried out. The PCR products

were purified by PCR SV gel and PCR cleanup kit (Promega). TOPO cloning was performed by following the manufacturer's instructions (Invitrogen). Normally 10 minipreps were set up per sample and sequenced. The PCR primers are listed in **Supplementary Table 3**. The PCR conditions used were as described[7].

Neuronal DNA isolation. We followed the protocol as described[48] to isolate the nuclei from adult forebrain (cortex and hippocampus). The nuclei were then dissociated and tagged by a NeuN antibody that was already incubated with an anti-mus IgG (Alexa 488) antibody. We then ran the fluorescent nuclei through a FACS machine (BD Biosciences) with proper gate settings. A small portion of the $NeuN^+$ nuclei were re-run on the FACS machine to validate the purity. Immunonegative ($NeuN^-$) nuclei were collected in parallel. The nuclei were then harvested by centrifuge and lysed for DNA under regular protocol.

Quantification of total methylcytosine using tandem mass spectrometry. The DNA hydrolysis protocol was as described[49]. Typically, 1 μg of genomic DNA was denatured (100 °C, 3 min). A 1/10 volume of 0.1 M ammonium acetate and 2 units of nuclease P1 (Roche) were added and incubated at 45 °C for 2 h. Then a 1/10 volume of 1 M ammonium bicarbonate and 0.002 units of venom phosphodiesterase I (Sigma) were added followed by another incubation (37 °C, 2 h). Subsequently, 0.5 units of alkaline phosphatase (Fermentas) was added, and the mixture was incubated at 37 °C for another 1h. LC-ESI-MS MS was performed as described[50] with some modifications[2]. DNA hydrolysis samples (20 μl) were injected onto a reverse phase HPLC column (Aquasil C18 2.1 × 200 mm, 5 μ particle size, Thermo Scientific) with a flow rate of 220 μL min^{-1} and equilibrated in buffer A (0.1% formic acid in water v/v). Elution was made by an increasing concentration of buffer B (0.1% formic acid in methanol v/v). The effluent from the column was directed to an electrospray ion source connected to a triple quadrupole mass spectrometer (AppliedBiosystems 4000Q Trap) operating in the positive ion multiple reaction monitoring mode using previously optimized conditions, and the intensity of specific $MH^+ \rightarrow$fragment ion transitions was recorded (5mdC *m/z* 242.1→126.1 and dC *m/z* 228.1→112.1). The 5mdC content in each sample was calculated from the MRM peak area by extrapolation from the response obtained following injection of known quantities of the authentic compound and expressed as a percentage of the total cytosine pool assuming equivalent molar responses.

Methylated DNA immunoprecipitation and microarray experiment (MeDIP-chip). Genomic DNA (2 μg) from 3-month-old DKO and control littermate forebrain tissue was sonicated to an average size of 350–400 bp. We added 20 μg mouse anti–5-methyl-cytosine antibody (Eurogentec) to the DNA samples and rotated them at 4 °C overnight. We washed 100 μl Dynabeads M-280 sheep anti-mouse IgG beads with FB buffer (10mM Tris-HCl, pH 7.5; 50mM NaCl; 1mM EDTA) and added them to the DNA-antibody mixture and rotated them at 4 °C for 8 h. The beads were washed four times with FB buffer, one time each with FB containing 150 mM or 300 mM NaCl. Serial elutions with 200 μl FB buffer of 1.5% SDS, 0.5% SDS and 0.1% SDS were made. All three elutions were pooled together and the DNA was purified by using phenol/chloroform. The eluted DNA was resuspended in water. The BioPrime array CGH genomic labeling kit (Invitrogen) was used to label equal amounts of pull down DNA with Cy5 (control) or Cy3 (KO). Agilent mouse promoter array hybridization was set up as described[30].

Statistical analysis. Data are presented as mean ± s.e.m. Unless otherwise noted, the Student's *t*-test (two-tailed) and the two-way ANOVA test were used for statistical analysis. Statistical significance was determined at $P < 0.05$.

43. Dodge, J.E. *et al.* Inactivation of Dnmt3b in mouse embryonic fibroblasts results in DNA hypomethylation, chromosomal instability, and spontaneous immortalization. *J. Biol. Chem.* **280**, 17986–17991 (2005).
44. Han, Y.G. *et al.* Hedgehog signaling and primary cilia are required for the formation of adult neural stem cells. *Nat. Neurosci.* **11**, 277–284 (2008).
45. Lu, X.H. *et al.* Bacterial artificial chromosome transgenic mice expressing a truncated mutant parkin exhibit age-dependent hypokinetic motor deficits, dopaminergic neuron degeneration, and accumulation of proteinase K-resistant alpha-synuclein. *J. Neurosci.* **29**, 1962–1976 (2009).
46. Cui, L. *et al.* Transcriptional repression of PGC-1alpha by mutant huntingtin leads to mitochondrial dysfunction and neurodegeneration. *Cell* **127**, 59–69 (2006).
47. Ethell, I.M. *et al.* EphB/syndecan-2 signaling in dendritic spine morphogenesis. *Neuron* **31**, 1001–1013 (2001).
48. Jiang, Y., Matevossian, A., Huang, H.S., Straubhaar, J. & Akbarian, S. Isolation of neuronal chromatin from brain tissue. *BMC Neurosci.* **9**, 42 (2008).
49. Crain, P.F. Preparation and enzymatic hydrolysis of DNA and RNA for mass spectrometry. *Methods Enzymol.* **193**, 782–790 (1990).
50. Song, L.J.S., Kazim, L. & Karpf, A.R. Specific method for the determination of genomic DNA methylation by liquid chromatography-electrospray ionization tandem mass spectrometry. *Anal. Chem.* **77**, 504–510 (2005).

doi:10.1038/nn.2514